Cellular Immunology 338 (2019) 51–62

Contents lists available at ScienceDirect

Cellular Immunology

journal homepage: www.elsevier.com/locate/ycimm

Poly(acrylic acid)-Coated Iron Oxide Nanoparticles interact with mononuclear phagocytes and decrease platelet aggregation

Manuela Giraldo Villegas[a], Melissa Trejos Ceballos[a], Jeaneth Urquijo[b], Elen Yojana Torres[a,c], Blanca Lucía Ortiz-Reyes[a], Oscar Luis Arnache-Olmos[b], Mauricio Rojas López[a,c,*]

[a] Grupo de Inmunología Celular e Inmunogenética, Sede de Investigación Universitaria (SIU), Universidad de Antioquia (UDEA), Calle 70 No. 52-21, Medellín, Colombia
[b] Grupo de Física del Estado Sólido, Sede de Investigación Universitaria (SIU), Universidad de Antioquia (UDEA), Colombia
[c] Unidad de Citometría de Flujo, Sede de Investigación Universitaria (SIU), Universidad de Antioquia (UDEA), Colombia

A B S T R A C T

Poly(acrylic acid)-Coated Iron Oxide Nanoparticles (PAC-IONs) did not compromise the viability of mononuclear cells and potentially interact with cells through scavenger receptors. This study evaluated: 1) The capacity of the PAC-IONs to induce platelet activation and aggregation, and 2) The effect of the PAC-IONs in two functions of Monocyte-Derived Macrophages (MDMs) when differentiated in their presence; that is, the removal of apoptotic cells (ACs) and the levels of cytokines induced by Lipopolysaccharide (LPS) and the ACs.

The PAC-IONs did not affect the platelet activation but antagonized their aggregation. On the other hand, the differentiation of MDMS in the presence of PAC-IONs did not inhibit the ability of these cells to phagocytose latex beads but decreased the number of apoptotic bodies internalized by them. MDMs differentiated in the presence of PAC-IONs and stimulated with LPS or ACs exhibited an overall decrease of the cytokine levels. The altered synthesis of cytokines could be attributed to a high production of Reactive Oxygen Species (ROS) caused by the increase in the intracellular iron content. The effect of the PAC-IONs on the cell cycle of U937 and Jurkat cells was also studied; there was not either cell accumulation in any phase of the cell cycle or changes in the DNA content.

It is clear that PAC-IONs affect neither the viability nor compromise some cellular functions. However, they could alter the functioning of the immune system; therefore, in the case of being used as a diagnostic tool, their permanence in the body should be considered.

1. Introduction

Poly(acrylic acid)-Coated Iron Oxide Nanoparticles (PAC-IONs)[1] interact with the surface of monocyte, possibly through scavenger receptors [1]. We have considered PAC-IONs as a potential noninvasive interface to track monocytes during the inflammatory processes. Monocytes are cells of the innate immune system and one of the bridges with the adaptive immune responses. That is why the understanding of the reactions of mononuclear phagocytes with PAC-IONs is critical before any possible application could be implemented in the study and treatment of human pathologies.

Conventionally, human monocytes are classified into subpopulations according to the surface expression of CD14 –the lipopolysaccharide (LPS) co-receptor– and CD16 –the low-affinity FcγRIII receptor involved in recognition of the immune complexes [2]. In 2010, an International Consortium under the auspice of the International Union of Immunological Societies (IUIS) and the World Health Organization (WHO) proposed nomenclature for monocyte subpopulations [2]. More recently, based on the Slan [3–5] and Tie-2 [6–8] expression, new monocytes have begun to be described. However, there is not a consensus about their specific roles in different pathologies.

For several years, one of the main interests of our Group has been the understanding of the role of monocytes in the immune response in some pathologies such as infection by *Mycobacterium tuberculosis* and Systemic Lupus Erythematosus (SLE). Our results involved the innate response in the murine model [9–13], the different mechanisms of cell death induced by *M. tuberculosis* in patients versus healthy controls [14]; the altered expression of molecules that are critical in the function of monocytes as Antigen-Presenting Cells (APCs) [15]; and, mainly, the increase in a cell subpopulation known as non-classical monocytes [16]. This cellular subset is more prone to cell death by infection with *M. tuberculosis* [17], is considered pro-inflammatory by some authors [18,19], destroy tissues in arthritis [20], and has higher ability to interact with the vascular endothelium [21]. In addition, different reports have shown an abnormal count of this cellular subset in pathologies such as those associated with the human immunodeficiency virus (HIV), parasitosis, atherosclerosis, arthritis, SLE, the Kawasaki syndrome, and heart disease [22]. In summary, it is clear that non-classical monocytes can infiltrate and mediate the tissue damage [23,24]. Notwithstanding, it should be stress that tissue damage is evident very late

* Corresponding author at: Unidad de Citometría de Flujo, Sede de Investigación Universitaria (SIU), Universidad de Antioquia (UDEA), Colombia.
E-mail address: mauricio.rojas@udea.edu.co (M.R. López).

[1] PAC-IONs: Poly(acrylic acid)-Coated Iron Oxide Nanoparticles

https://doi.org/10.1016/j.cellimm.2019.03.005
Received 17 December 2018; Received in revised form 18 March 2019; Accepted 25 March 2019
Available online 26 March 2019
0008-8749/

in the course of a disease when treatments are just palliative. Invasive methods as biopsies can be used to establish the type and degree of damage, but there are not early biomarkers for predicting its progression. Therefore, the *in vivo* tracking, detection, and manipulation of monocytes in the inflammatory sites has become an alternative. The early detection of monocytes in the tissues could favor the prognosis and the targeted-intervention of patients of multiple diseases.

Detection of tissue phagocytes by extracorporeal imaging is possible when a large number of cells have accumulated at such a level that the effects of the lesion are not reversible. The gadolinium derivatives are currently used as contrast media, but they are toxic [25–29], nephrotoxic [30,31], immunogenic, allergenic [32–36], and very expensive. Also and despite the low emissions, they involve radio-labeling at levels that are not entirely harmless for cells and tissues, like in the positron emission tomography [37]. Some of the current techniques described above also require a costly infrastructure to generate the radioactive material.

The above concerns have encouraged the search for a nanosensor that interacts with the mononuclear phagocytes. This nanosensor would be intended to differentially interact with the monocyte subsets, allowing this way their *in vivo* identification. Also, this magnetic nanosensor should be "innocuous" although its innocuousness could not be related exclusively with cell viability, but the physiology of the phagocytes, specifically their differentiation. Additionally, the physical and magnetic properties of the nanosensor should be kept stable during the *in vivo* tracking process.

We have considered the use of PAC-IONs with a hydrodynamic diameter of 20–25 nm as nanosensors. Some of their effects could be explained by the putative interactions of their coating with the cellular Scavenger Receptors (SRs). Previous studies have shown that the conjugation of liposomes with polyacrylate increases their endocytosis, although their uptake decreases by competition with SR ligands such as acetylated-low density lipoproteins (acLDL) and dextran sulfate [1]. Also, our current studies indicated that monocyte-derived macrophages (MDMs), when differentiated in the presence of PAC-IONs, showed a lower expression of the SR CD36 than the MDMs not exposed to the nanoparticles during their differentiation.

The present study aimed to evaluate the biosafety of PAC-IONs. Specifically, interactions of the nanoparticles with circulating monocytes and platelets were evaluated. These cells share the expression of some SRs such as CD36, SR-B1, and LOX-1 [38]. The activation and aggregation of platelets in the presence of PAC-IONs and a commercial source of iron nanoparticles (carboxylic acid functionalized, 5 mg/mL Iron (II, III) – CA-IONs-[2]) were evaluated, as well as the changes in functional characteristics of mononuclear phagocytes such as the phagocytosis of apoptotic cells (ACs) and the cytokine production in response to lipopolysaccharide (LPS) and ACs. PAC-IONs did not alter platelet activation or aggregation but did antagonize the platelet aggregation induced by Phorbol Myristate Acetate (PMA) or arachidonic acid (AA). On the other hand, the differentiation of MDMs in the presence of PAC-IONs did not reduce the number of MDMs that phagocytosed ACs, but the number of ACs internalized per cell. Overall, the MDMs differentiated in the presence or not of PAC-IONs showed reduced production of cytokines. However, TNF-α increased in the cultures of MDMs differentiated in the presence of the nanoparticles but not stimulated with LPS or ACs.

The present findings are starting points for future research intended for warranting the use of PAC-IONs as nanosensors. These particles should have superparamagnetic properties, be selective for mononuclear phagocytes or their subpopulations, and produce few side effects. The PAC-IONs could be a useful tool for characterization of early-stage tissue lesions and the understanding of the role of monocytes and macrophages in different immunopathologies.

[2] CA-IONs: 10 nm avg. part. size (TEM), carboxylic acid functionalized, 5 mg/mL Iron (II, III) dispersed in H_2O

2. Materials and methods

2.1. Materials

Brain Heart Infusion (BHI) broth, anti-CD41a (CD41/CD61 GPIIb/IIIa complex) (anti-CD41a-PE, clone HIP8), anti-P selectin (anti-CD62P-PECy-5, clone AK-4), anti-CD14 (clone MφP9) monoclonal Antibodies (mAbs), Annexin V-PE, 0.105 M sodium citrate tubes, and the CBA Human Inflammatory Cytokines Kits were purchased from BD Biosciences (San Jose, CA). Limulus Amebocyte Lysate (LAL) was obtained from LONZA (Visp, Switzerland). Gentamicin, PMA, Dimethyl Sulfoxide (DMSO), 1.077 g/mL Histopaque, trypan blue, LPS and 10 nm avg. part. size (TEM), carboxylic acid functionalized, 5 mg/mL Iron (II, III) dispersed in H_2O were obtained from Sigma-Aldrich (St. Louis, MO). Colchicine was got from Winthrop Pharmaceuticals (Sanofi; Bridgewater, NJ). RPMI-1640-Glutamax-Streptomycin-Penicillin, Phosphate Buffered Saline (PBS) were purchased from Gibco-BRL (Thermo Fisher Scientific, Waltham, MA). Hoechst 33342, 3,3′-dihexyloxacarbocyanine Iodide ($DIOC_6$), and propidium iodide (PI) and Paraformaldehyde were purchased from Invitrogen (Thermo Fisher Scientific; Waltham, MA). Sterile glass spheres of 5 mm diameter and 48-well flat bottom plates were obtained from Pyrex-Corning (Sigma-Aldrich, St. Louis, MO, USA). The tuberculin syringes were got from Rymco (Barranquilla, Colombia). The TUNNEL (Terminal-Deoxynucleotide-Transferase (TdT) dUTP-Biotin Nick End Labeling) assay was obtained from MEBSTAIN (Medical and Biological Laboratories Co., Ltd., Nagoya, Japan).

2.2. Study population

Peripheral blood samples were taken from healthy adults working at the Research Headquarters of the Universidad de Antioquia. They declared not having either coagulation, autoimmune or active infectious diseases. They voluntarily agreed to participate in the research and signed an informed written consent, approved by the Ethics Committee of the Instituto de Investigación Médica.

2.3. Nanoparticles synthesis

PAC-IONs were prepared through the coprecipitation method, according to Lin et al. [39], in the Grupo de Estado Sólido of the Instituto de Física at Universidad de Antioquia. Briefly, Magnetic magnetite-maghemite particles were obtained by coprecipitation from an aqueous alkaline solution of $FeCl_2.4H_2O$ and $FeCl_3.6H_2O$ (1:2 stoichiometric ratio) in the presence of 0.4% (w/w) sodium polyacrylate as a stabilizing agent. The pH was adjusted to 12 with the automatic addition of 1 M NaOH, using a 907 Titrando, (Metrohm; Herisau, Switzerland). Previous to the synthesis procedure, solutions were passed under an N_2 (g) flow. During the synthesis, the N2 (g) flow was kept constant to avoid oxidation of the oxide particles after their formation. The precipitate obtained was dialyzed with a Spectra/Por® 100 kDa MWCO cellulose membrane (Molecular Weight Cut Off. Vacaville, CA) against type II deionized water, until the conductivity of the washing water was similar to that of the deionized water. An aliquot of the particle suspension was stored at room temperature for *in vitro* analyses, and another one was vacuum dried at room temperature and stored in an N_2 atmosphere for further assays.

Morphological, physical, and chemical characteristics of PAC-IONs were evaluated by different methods. The hydrodynamic particle diameters, size distribution, and zeta potential were measured by Dynamic Light Scattering (DLS) with Zetasizer equipment (Malvern Panalytical; Almelo, The Netherlands) at room temperature. To this purpose dried PAC-IONs were resuspended (1 mg/10 mL) in a 50:50 (v/v) ethanol-water mixture for a triplicate analysis of size distribution. Another

suspension of PAC-IONs (0.5 mg/10 mL) in water was used for evaluating the zeta potential with the Smoluchowski equation. Additionally, the ethanol–water suspension was utilized for analyzing morphology by Transmission Electron Microscopy (TEM) with a JEOL 100-CX II microscopy (Jeol Ltd; Tokyo, Japan).

The magnetization of PAC-IONs was determined in a sample of dried particles under an applied magnetic field with a Physical Property Measurement System (PPMS) (Quantum design; San Diego, CA), using the VSM module and an −0.5 T to 0.5 T scan at room temperature (300˚K).

2.4. Isolation of platelets

Peripheral blood samples were drawn in 0.105 M sodium citrate tubes and centrifuged at 240 × *g* for 20 min and 20 °C for obtaining Platelet-Rich Plasma (PRP). Then, a fraction of PRP was centrifuged at 10,000 × *g* for 5 min and 20 °C for getting Platelet-Poor Plasma (PPP) [40]. PRP was diluted 10X and 5X for the activation and the aggregation assays, respectively. The presence of platelets was determined by staining the samples with anti-CD41a-PE mAb. The PPP was used to define the FSC-A threshold and avoid recording dust, cell debris, or electronic noise during the samples acquisition in a FACSCanto II Flow Cytometer (BD Biosciences). Forward scatter-height (FSC-H) versus FSC-area (FSC-A) dot plots were used for excluding the aggregates.

2.5. Platelet activation assay

The PAC-IONs were suspended in RPMI-1640 without serum at concentrations from 1 to 64 μg/mL, according to a prior viability test with peripheral blood cells. Fifty μL of the PAC-IONs suspension was mixed with 50 μL of the 10X-diluted PRP. Then, the platelet activation was evaluated by staining the P-selectin exposed on the cell membrane of platelets, with anti-CD62P-PECy-5 mAb. PMA was used as a positive control (2.5 μg/mL, previous standardization by flow cytometry), and PBS as the negative one.

2.6. Aggregometry

PRP (288 μL) was diluted 2X in PBS and incubated for 30 min at 37 °C with (i) PBS, (ii) 2.5 μg/mL PMA, (iii) 0.5 μg/mL AA, (iv) PAC-IONs, or (v) a combination of PAC-IONs with antagonists. Subsequently, the diluted-PRP was re-calcified (final concentration 2.5 mM $CaCl_2$). Platelet aggregation was recorded for 7 min while stirring using an MCM HEMA-TRACER 212 aggregometer (MC Medical, Tokyo, Japan). Light transmission was adjusted to 0% transmittance (%T) with PRP and 100 %T with PPP for each measurement. Platelet aggregation was determined as the maximum change in the %T from the baseline, using the PPP as a reference.

2.7. Generation and labeling of apoptotic Jurkat cells

Jurkat cells (ATCC TIB-152) were cultured in RPMI-1640 supplemented with Glutamax, 5% inactivated Fetal Calf Serum (iFCS), 100 mg/mL streptomycin, and 100 IU/mL penicillin. For obtaining apoptotic cells (ACs), 1×10^7 Jurkat cells were resuspended in 13 mL of supplemented RPMI, exposed to 0.1 μM colchicine in DMSO, and incubated at 37 °C and 5% CO_2 for 24 h. (51). After, the cells were centrifuged at 1000 × *g* for 10 min; the supernatant was discarded, and the ACs were washed with 13 mL of PBS to eliminate the colchicine residues. Then, 2 mL of a buffered solution (Hanks' balanced salt solution, 2 mM Hepes and 2% FCS) and Hoechst 33342 (final concentration 5 μg/mL) were added. After, 3 mL of the buffered solution containing $DIOC_6$ (final concentration 70 nM) and PI (final concentration 2.8 μg/mL) were added. Hoechst 33342, $DIOC_6$, and PI were used for evaluating the DNA content, mitochondrial membrane potential (ΔΨm) and cell membrane integrity, respectively. Finally, $DIOC_6^{low}$ (low mitochondrial membrane potential), PI^{neg} (no cell membrane damage), and $Hoechst^{low}$ (hypoploid) cells were chosen for electromagnetic sorting using a MoFlo™ XDP Cell Sorter (Beckman & Coulter; Fort Collins, CO). In all cases, efficiency and purity were 95%. The ACs were tested and used immediately.

2.8. The phenotype of the sorted ACs

Sorted apoptotic Jurkat cells (5×10^5) were resuspended in 200 μL of Annexin V-binding buffer (0.1 M HEPES pH 7.4, 1.4 M NaCl, 25 mM $CaCl_2$), stained with 5 μL of Annexin V-PE and 10 μg/mL PI, incubated in darkness for 30 min at room temperature and acquired in the flow cytometer to determine the phosphatidylserine exposure on the cell membrane. A control without Annexin V was set in parallel. Also, an aliquot of ACs was used to detect the presence of DNA breaks by the TUNEL assay using a commercial kit following the manufacturer's instructions. Briefly, the cells were washed with PBS, fixed with 4% paraformaldehyde, and permeabilized by the addition of 200 μL of 0.5% Tween 20 with 0.2% BSA in PBS. The enzymatic TdT reaction was carried out in the presence of FITC-dUTP for 30 min at 37 °C to reveal the DNA breaks. As a negative control, all the reagents were added under the same conditions, but without the TdT enzyme. Then, cells were acquired in a flow cytometer for detecting the FITC fluorescence.

2.9. Peripheral blood mononuclear cells (PBMCs) and mononuclear phagocytes

PBMCs were isolated from 10 mL of EDTA-anticoagulated blood samples by centrifugation on Histopaque density (1.077 g/mL) gradient at 900 × *g* for 30 min. PBMCs were washed with PBS and washing buffer (PBS plus 1% BSA and 0.1% NaN_3) and resuspended in staining buffer (PBS plus 1% pooled human serum (PHS)). Viability was ≥98% as determined by trypan blue dye exclusion.

2.10. Isolation of monocytes and differentiation into macrophages

Sixty mL of peripheral blood was defibrinated in an Erlenmeyer containing 25 sterile, glass beads 5 mm in diameter (Pyrex; Corning, NY). Then, PBMCs were isolated by centrifugation on a Histopaque density (1.077 g/mL) gradient at 900 × *g* for 30 min at room temperature. PBMCs were recovered and washed twice with PBS. The percentages of $CD14^+$ monocytes in the isolated PBMCs were determined by labeling 3.0×10^5 cell/μL with 5 μL of anti-CD14-PE mAb (Clone: 322A-1 (MY4) Beckman Coulter Company). Then, 2.5×10^5 or 7.5×10^4 $CD14^+$ cell/well were plated in 48- or 96-well dishes at a final volume of 500 and 200 μL, respectively. The cells were cultured in media containing 0.5% FCS at 37 °C and 5% CO_2 and allowed to adhere to plastic. After 4 h of incubation, the monolayer was washed with PBS containing 0.5% FCS at 37 °C to remove non-adherent cells followed by verification under an inverted microscope [16]. Then, adherent cells were cultured for 120 h until differentiated into macrophages in the presence or absence of 32 μg/mL of PAC-IONs. The cell purity of the Monocyte-Derived Macrophage Monolayers (MDMMs) was determined on the fifth day of differentiation by staining with fluorescent Mouse Anti-Human PerCP-CD3 (clone OKT3), Alexa Fluor® 488 CD19 (clone HIB19) and BV510 CD56 (clone NCAM16.2) mAbs (BD Biosciences) to identify the presence of contaminant T, B, and NK-cells, respectively. In all cases, the cell purity of the MDMMs was higher than 95% by flow cytometry.

In order to establish the biocompatibility of the PAC-IONs, dose-response tests were performed using human mononuclear phagocytes. Briefly, isolated mononuclear phagocytes were incubated for 120 h with the nanoparticles (diluted in RPMI supplemented with 10% inactivated autologous serum) in the following gravimetry-estimated-iron content: 6.2, 12.4, 18.6, 24.8 and 31 μg.

2.11. Differentiation profile of MDMs

Monocyte-derived macrophages differentiated in the presence or absence of PAC-IONs (3×10^5) were stained with Fluorescein Diacetate (FDA) [41] and fluorescent conjugated mAbs against HLA-II, CD14, HLA-DR, CD80, CD206, CD36, CD163, CD40, CD119, and CD64. Matched isotype mAbs were used as negative controls. Cells were fixed with 2% paraformaldehyde for 20 min, washed and scrapped with a rubber policeman. Ten thousand events were analyzed by flow cytometry.

For intracellular CD68, 5×10^5 cells were stained with anti-HLA-II-FITC, incubated for 30 min at room temperature, and washed with 1% BSA in PBS. Then, cells were fixed with 2% paraformaldehyde for 20 min, permeabilized with a saponin solution (0.1% Saponin 1% BSA in PBS). After, cells were stained with anti-CD68-PE or the respective isotype mAb control for 30 min at room temperature and washed twice. Samples were acquired in the LSRFortessa II™ flow cytometer (BD Biosciences).

2.12. Acridine orange (AO) and propidium iodide (PI) for cell viability

Acridine orange is an intercalating dye that can permeate both live and dead cells. AO stains all nucleated cells to generate green fluorescence and PI can only enter dead cells with poor membrane integrity, so it will stain all dead nucleated cells to generate red fluorescence. Cells stained with both AO and PI fluoresce red due to quenching, so all live nucleated cells fluoresce green and all dead nucleated cells fluoresce red. Thus, 1 µL Acridine Orange Stock (5 µg/mL) and 1 µL PI Stock (3 µg/mL) were added to culture plates and cells were analyzed under an inverted fluorescent microscope Olympus CKX53 (Richmond Hill, Ontario).

2.13. Gating of MDMs to evaluate phagocytosis

The evaluation of phagocytosis of ACs by MDMs required the gating of an optimal MDM region to distinguish them from the cellular aggregates (containing PAC-IONs) and the free apoptotic bodies (without making additional stains that affected the interaction of MDMs with the apoptotic Jurkat cells). To this purpose, in an independent assay, cells were stained with anti-CD36 and anti-HLA-DR mAbs to gate the $CD36^{high}HLA\text{-}DR^{high}$ MDMs. From this gate, an SSC-A versus FSC-A dot plot was drawn to build a region named "MDM." SSC-A versus FSC-A dot plots were also drawn for ACs. An overlay of the dot plots showed that the proposed "MDM" region was appropriated for the evaluation of phagocytosis.

2.14. Phagocytosis of latex beads and apoptotic Jurkat cells

After 120 h of differentiation, MDMs were incubated with fluorescent latex beads at 1:1 and 5:1 ratios (MDM: bead) or with ACs at 1:1 and 1:2 ratios (MDM: ACs). The MDM-AC junction was synchronized by centrifugation of dishes at $1000 \times g$ for 5 min followed by incubation for 2 h at 37 °C and 5% CO_2. Then, MDMs were detached with the plunger of a tuberculin syringe and analyzed by flow cytometry to evaluate both the $DIOC_6{}^+$ ACs bound to and phagocytosed by the MDMs. Finally, a second acquisition was performed on the same tube, after adding 5 µL of 0.4% trypan blue, to quench the peripheral $DIOC_6$ fluorescence of the ACs that had not been internalized.

2.15. Cytokines in cultures of MDMs (differentiated in the presence of PAC-IONs) exposed to apoptotic cells

Monocyte-derived macrophages differentiated in the presence of PAC-IONs were incubated with ACs at 1:1 and 1:2 ratios (MDM:AC) and 0.1 µg/mL of LPS for 4 and 24 h, respectively. The dishes were centrifuged at $1000 \times g$ for 7 min, and the supernatants were collected. The levels of IL-8, IL-1β, IL-6, IL-10, TNF-α, and IL-12p70 were measured by CBA and flow cytometry according to the manufacturer's instruction.

2.16. The cell cycle of U937 and Jurkat cells exposed to PAC-IONs

The human promonocytic U937 (ATCC CRL-1593) and the lymphoid Jurkat, Clone E6 (ATCC TIB-152) cells were cultured in RPMI supplemented with 5% FCS. Then, 100,000 cells/well were seeded in 48-well dishes and incubated with PAC-IONs (31 µg of iron) at 37 °C and 5% CO_2 for 24, 48 and 72 h. After, the dishes were centrifuged at $600 \times g$ for 5 min, the medium was removed, and the cells were washed with cold PBS and fixed with cold 70°GL ethanol for 24 h. Then, cells were washed with PBS and stained with 300 µL of PI/RNase (30 IU/mL) [42] (BD Biosciences) for 30 min at room temperature. Finally, cells were acquired in a FACSCanto II Flow Cytometer to analyze the relative content of DNA.

2.17. Analysis of data

Flow cytometry data were analyzed with the Kaluza software version 1.2 (BeckmanCoulter) and FlowJo software version X (TreeStar Inc.; Ashland, OR). The statistical analyses were performed with the Statgraphics Centurion 16.1.18 (StatPoint Technologies Inc; Warrenton, VA) and the GraphPad Prism software version 5.0 (Graphpad Software Inc; San Diego, CA). The mean fluorescence intensity (MFI) values and percentages of positive cells from paired treatments were compared with the Wilcoxon test, and the cytokine concentrations with a two-way ANOVA, with a Bonferroni post-test. Values of $p < 0.05$ and < 0.01 were set as statistically significant. Histograms were compared using the Overton subtraction in the FlowJo software.

3. Results

Initially, the cytotoxic effect of several concentrations of PAC-IONs (from 6.2 to 31 µg iron, quantified by gravimetry) upon mononuclear phagocytes was tested; viability results were similar to previous reports [43]. In the present study, also the effect of PAC-IONs and CA-IONs on the macrophage differentiation was evaluated. Adherent monocytes were exposed to PAC-IONs and CA-IONs, and allowed to differentiate for 120 h [44]. Then, cell death was assessed by staining with $DIOC_6$ and PI [14]. There were no changes either in the percentage of PI^+ and $DIOC_6{}^+$ cells or the $DIOC_6$ MFI, indicating that the PAC-IONs did not affect the viability of MDMs during their differentiation (data not shown). Uncoated nanoparticles, in the same concentration range, induced cell membrane damage at 12.4 µg/mL. This result indicated the relevance of the coating in the interaction with mononuclear phagocytes. Therefore, MDMs were stained with AO and PI and analyzed under a fluorescence microscope. The evaluation confirmed that the PAC-IONs and CA-IONs were not toxic for the mononuclear phagocytes. The microphotographs showed that in contrast to the uncoated nanoparticles, the PAC-IONs and CA-IONs seemed to have been internalized by the cells. The uncoated nanoparticles were toxic for the phagocytic cells at concentrations above to 12.4 µg/mL (Fig. 1).

3.1. PAC-IONs did not induce P-selectin exposure and inhibited the platelet aggregation

As previously described, the highest concentration of PAC-IONs and CA-IONs here evaluated (31 µg/mL) did not cause the death of either PBMCs or monocytes. After, the objective was to analyze whether 31 µg/mL of PAC-IONs and CA-IONs could induce the P-Selectin (CD62P) exposure on the surface of platelets. When intracellular alpha granules are released –an event that is usually interpreted as a first activation signal– CD62P is exposed on the platelet membrane [45]. Platelets exposed to 31 µg/mL of PAC-IONs did not show any change in surface CD62P; however, when those platelets were treated with PMA the CD62P MFI increased in 6 out of 6 trials ($p = 0.0206$) (Fig. 2C and

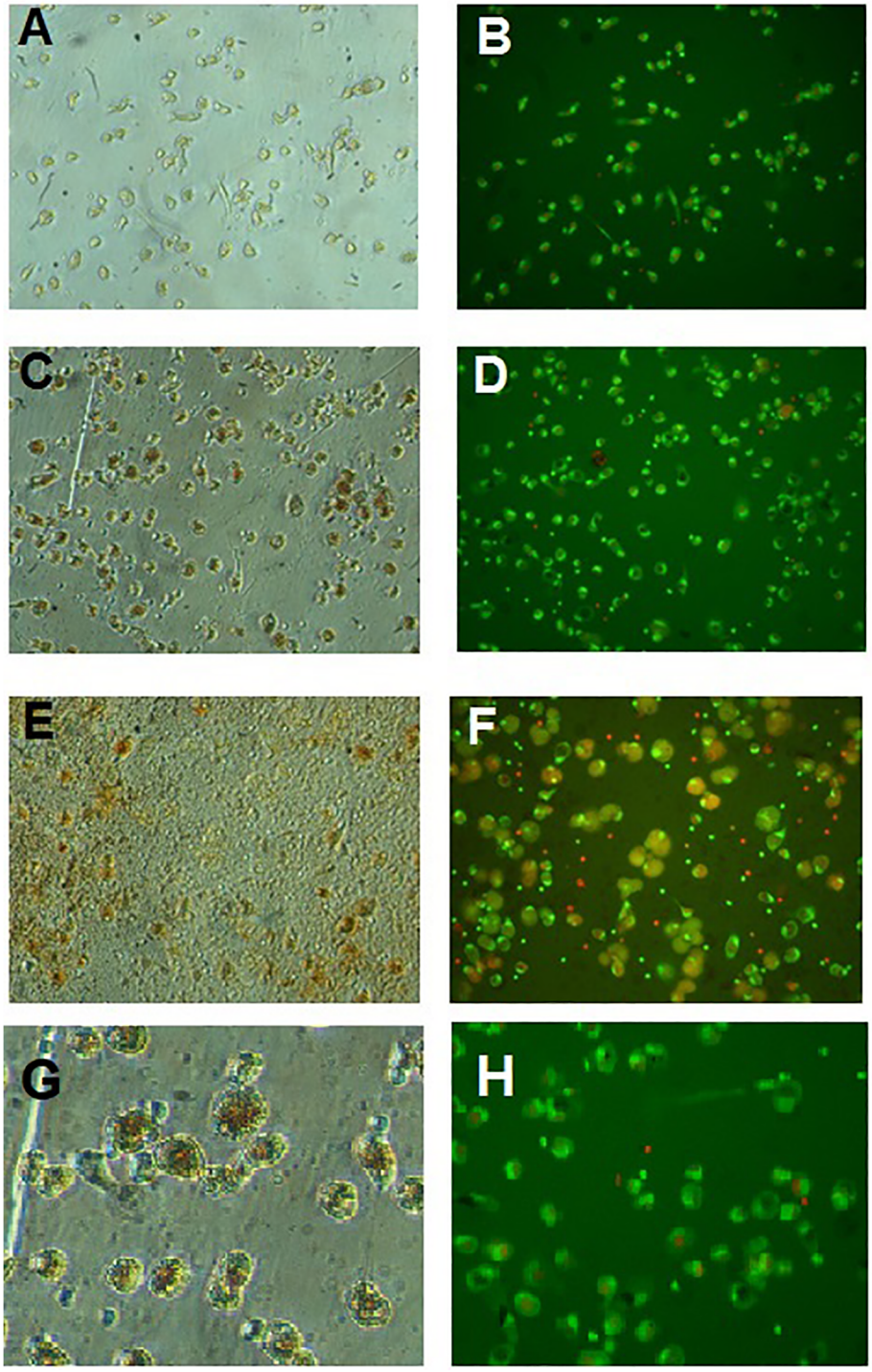

Fig. 1. PAC-IONs do not alter the viability of MDMs differentiated in their presence. Mononuclear phagocytes were plated and allowed to differentiate into macrophages during 120 h in the absence (A, B) or presence of 31 μg iron of PAC-IONs (C, D) or uncoated IONs (E, F) and 31 μg iron of CA-IONs (G, H). MDMs were stained with Acridine Orange and Propidium Iodide and analyzed under both an optical (A, C, E) and a fluorescence (B, D, F) microscope (40X or G and H 60X). No differences were observed between cultures differentiated in the presence (C, D) or absence of PAC-IONs (E, F); n = 5.

D). Surface CD62P did not change either in platelets exposed to 1 μg/mL to 62 μg/mL PAC-IONs compared to the non-exposed control (data not shown). Nevertheless, when platelets were exposed to CA-IONs (31 μg/mL), the expression of surface CD62P increased significantly ($p = 0.0015$, Fig. 2C and D).

The effect of PAC-IONs on platelets was also studied by Light Transmission Aggregometry. The %T of the platelets treated with PAC-IONs was very similar to that of the negative control, indicating that the PAC-IONs did not induce platelet aggregation (Fig. 2E). It should be noted that platelet aggregation was significantly reduced when PAC-IONs-exposed-platelets were stimulated with AA, PMA, or ADP (Fig. 2E). On the contrary, platelet aggregation increased slightly when CA-IONs-exposed-platelets were stimulated with PMA or ADP, and significantly in the presence of AA ($p < 0.001$) (Fig. 2E).

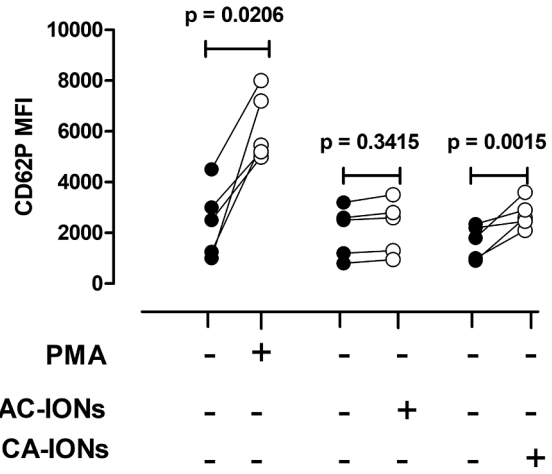

Fig. 2. Strategy to evaluate platelet activation. A PRP sample was treated for 20 min with PBS (non-stimulated), 2.5 μg/mL of PMA, or 31 μg/mL of PAC-IONs or 31 μg/mL CA-IONs; stained with fluorescent anti-CD41a-FITC and CD62P-PECy5 mAbs; and analyzed by flow cytometry. Doublets were excluded in an FSC-H versus FSC-A dot plot (A), and activated platelets were identified as $CD41a^+CD62P^+$ events (B). Histograms show the CD62P MFI of platelets treated with PBS (blue line), PMA (orange line), PAC-IONs (red line) or CA-IONs (green line) (C). CD62P MFIs were compared between the different groups; n = 6 independent experiments (D). Percentage of transmittance of non-exposed (black bars), PAC-IONs (white bars), or CA-IONs (hatched bars) -exposed platelets stimulated with PBS (NS), AA, PMA, or ADP; n = 5 independent experiments; $^{**}p \leq 0.01$, $^{*}p \leq 0.05$) (E).

3.2. Phagocytosis of ACs, but not of latex beads, by MDMs (differentiated in the presence of PAC-IONs) is reduced

Apoptotic Jurkat cells were obtained by treatment with 1 μM Colchicine according to previous reports from our Group [46]. The percentage of $DIOC_6^{low}$ PI- (Fig. 3A) and hypoploid (Fig. 3B) Jurkat cells oscillated between 40 and 70%. The electromagnetic separation of these apoptotic Jurkat cells had an efficiency of 95% and a purity greater than 95% in all cases (Fig. 3C).

After the electromagnetic separation, apoptotic Jurkat cells were tested by the Annexin V/PI and the TUNEL assays to verify the phosphatidylserine exposure on the cell membrane and the DNA damage, respectively. The percentage of Annexin V^+ ACs was between 70 and 100% (Fig. 3D). The percentage of $TUNEL^+$ ACs after the Overton histogram subtraction was between 30 and 70% (Fig. 3E and F). The ACs were used in the phagocytosis assays immediately after their electromagnetic sorting. For a suitable identification of the MDMs and exclusion of the free ACs, an "MDM" gate was defined based on cell granularity (SSC-A) and expression of HLA-DR. The $DIOC_6^+$ MDMs were MDMs that either attached ACs to their surface or internalized them. To distinguish bound and internalized ACs, samples were stained with trypan blue to quench the surface fluorescence. The results are presented as the $DIOC_6^+$ cells and the MFI as an indicator of the amount of ACs per MDM. The percentages of MDMs that had phagocytosed ACs were similar for cells differentiated or not in the presence of PAC-IONs (Fig. 4A and B). On the other hand, the amount of ACs internalized per MDM was lower for cells differentiated in the presence of the PAC-IONs than without them (Fig. 4C and D). Nevertheless, when the phagocytosis assay was performed with latex beads, no differences were observed between MDMs differentiated or not in the presence of PAC-IONs, suggesting that the decreased recognition and internalization of apoptotic bodies was a specific effect (data not shown). To note that the effect of CA-IONs was even stronger on percentage of DIOC6 + apoptotic bodies, as well as the uptake of the apoptotic bodies.

3.3. The PAC-IONs altered the CD36 expression of MDMs

Several parameters of MDMs (16, 46) were analyzed after their differentiation in the presence or absence of PAC-IONs for 120 h. Specifically, the hydrolysis of FDA and the expression per cell of HLA-DR, CD206, CD80, CD36, CD119, CD40, CD64 and CD163 were evaluated by flow cytometry. Comparisons between groups were made with the Wilcoxon test. The PAC-IONs only decreased significantly ($p < 0.0001$) the expression of CD36 (Fig. 5E). On the other hand, CA-IONs induced a significant decrease in the expression of HLA-DR (Fig. 5B) and CD36 (Fig. 5F).

3.4. Effect of LPS and ACs in the cytokine pattern of cultures of MDMs differentiated in the presence of PAC-IONs

Monocyte-derived macrophages differentiated in the presence or not of nanoparticles for 120 h were stimulated with 0.1 μg/mL LPS or ACs (at 1:1 and 1:2 ratios (MDM: AC)). Then, the accumulation of IL-1β, IL-6, IL-8, IL-12, TNF-α, and IL-10 was evaluated in the culture supernatant after 4 and 24 h. IL-12 was not detected in any case. The levels of IL-8 were quite homogeneous among all trials and treatments, but no differential effects were observed. The level of IL-1β was similar in cultures of MDMs differentiated or not in the presence of PAC-IONs and stimulated during 4 h with LPS or ACs (Fig. 6A–B). However, after 24 h, the level of IL-1β was significantly increased in response to LPS, and PAC-IONs but not CA-IONs, antagonized the accumulation of this cytokine (Fig. 6C and D). The nanoparticles alone did not induce IL-6. Compared with cultures differentiated in the absence of nanoparticles and stimulated with LPS, the presence of PAC-IONs significantly reduced LPS-induced IL-6 and in the presence of CA-IONs there was a significant increase at both time points (Fig. 6E and G). Negligible amounts of IL-6 were observed in response to CA at 4 h, and at 24 h it was observed an increase in the accumulation of this cytokines in response to both proportions of CA. This increase was significantly reduced in the presence of PAC-IONs, but not in the presence of CA-IONs (Fig. 6H).

The CA-IONs induced significant increase in the accumulation of TNF-α without any additional stimuli at 4 h and at 24 h both PAC-IONs and CA-IONs induced this TNF-α (Fig. 6I–L). At 4 h PAC-IONs antagonized LPS-induced TNF-α and CA-IONs significantly increased it. But at 24 h both nanoparticles increased LPS-induced TNF-α induced accumulation (Fig. 6I and K). To note, in the presence of CA, PAC-IONs antagonized TNF-a but CA-IONs increased the accumulation of this cytokine at both 4 and 24 h (Fig. 6J and L).

IL-10 was mainly induced with LPS at both time points, and its accumulation in the culture supernatants was decreased in the cultures of MDMs differentiated in the presence of PAC-IONs and CA-IONs and stimulated with LPS (Fig. 6M and O). IL-10 was detected in response to ACs at 24, and its increase was not significant due to the variability in the replicas, but this increase was also reduced in the presence of both nanoparticles (Fig. 6N and P).

3.5. The PAC-IONs did not affect the proliferation of Jurkat or U937 cells

The effect of PAC-IONs on the proliferation of lymphocytes, regardless of their effects on the mononuclear phagocytes, was indirectly analyzed by culturing the lymphoid Jurkat cells with nanoparticles for 24, 48 and 72 h. The PAC-IONs did not alter the cell cycle at 24, 48 (data not shown) and 72 h (Compare untreated cells in Fig. 7A and B). Besides, the cells did not show either FSC or SSC changes. Similarly, the PAC-IONs did not alter the cell cycle (Compare untreated cells in Fig. 7E and F) or FSC of U937 cells; however, the SSC changed, probably due to the PAC-IONs uptake. Conversely, the treatment of Jurkat and U337 cells with CA-IONs induced a significant accumulation of cells in G0/G1 (Fig. 7C and G; and consolidated bars from similar experiments, Fig. 7D and H). Additionally, Jurkat and U937 cells showed

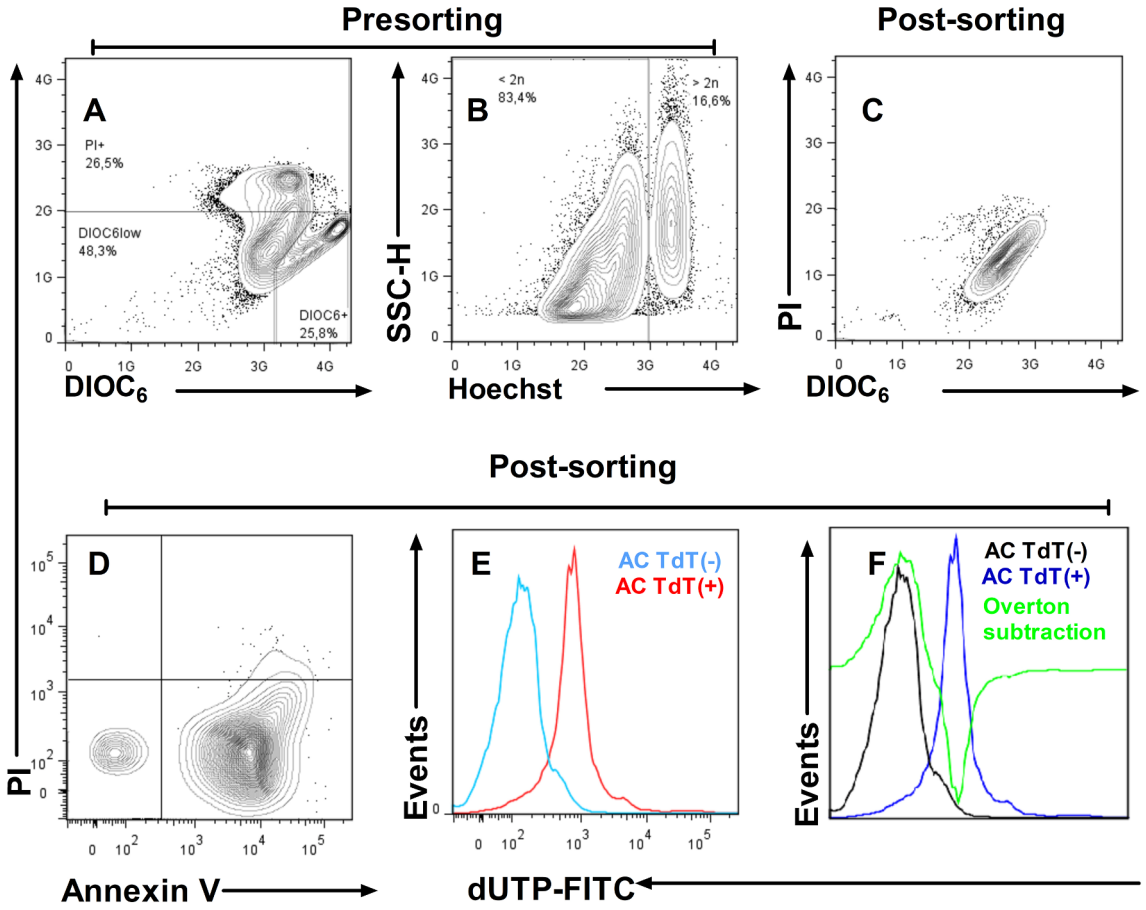

Fig. 3. Gating strategy for sorting and characterization of apoptotic Jurkat cells. Jurkat cells were treated with colchicine for 24 h and stained with $DIOC_6$, PI, and Hoechst dyes. $DIOC_6^{low}PI^{neg}$ (A) and $Hoechst^{low}$ (B) apoptotic cells were gated for sorting. The sorted $DIOC_6^{low}$ PI^{neg} apoptotic population reached a purity of 92% (C) and contained 66% of Annexin V^+ cells (D). A TUNEL assay confirmed the presence of TdT^+ cells (red histogram); control for TdT^{neg} cells (blue histogram) (E). The Overton subtraction was used for comparing the histograms of TdT^+ (blue) and the TdT^{neg} (black) cells. The green line represents the result of the Overton subtraction performed in the FlowJo software (F).

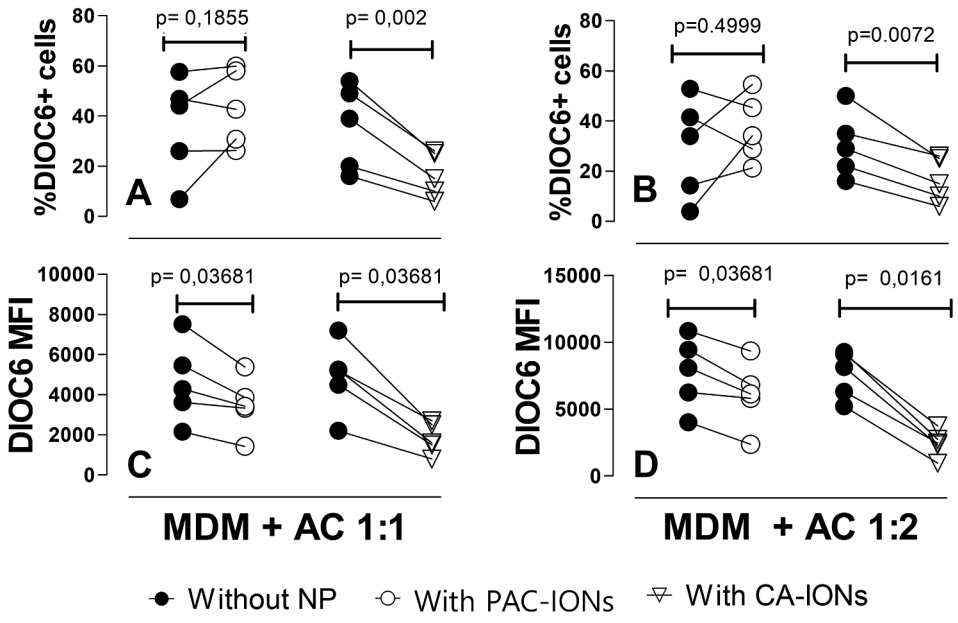

Fig. 4. The MDMs differentiated in the presence of PAC-IONs and CA-IONs phagocytosed fewer ACs per cell. MDMs differentiated in the absence (black circles), or presence of PAC-IONs (open circles) or CA-IONs (open triangles) for 120 h were incubated with ACs at 1:1 and 1:2 ratios (MDM: AC) for two hours. Percentages of MDMs that phagocytosed $DIOC_6^+$ ACs (A and B). $DIOC_6$ MFI of ACs internalized by the MDMs (ACs phagocytosed per MDM) (C and D). The Wilcoxon test was used for comparisons between groups; n = 5 independent experiments.

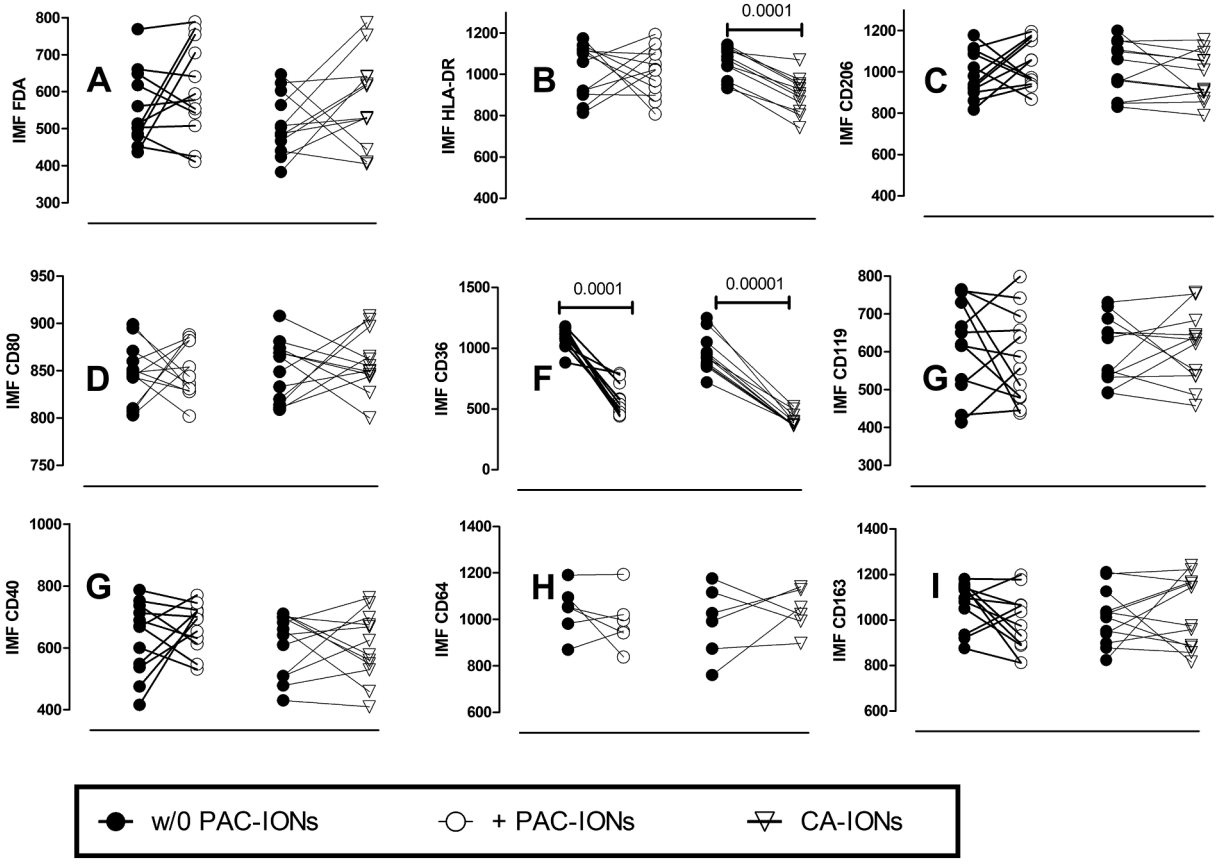

Fig. 5. Phenotype of MDMs differentiated in the presence of PAC-IONs and CA-IONs. MDMs differentiated in the absence (black circles) or presence of PAC-IONs (open circles) or CA-IONs (open triangles) for 120 h were stained with FDA, for evaluating non-specific esterases (A), or with fluorescent mAbs against several molecules related with cell differentiation, HLA-DR (B), CD206 (C), CD80 (D), CD36 (E), CD119 (F), CD40 (G), CD64 (H) and CD163 (I). Cells were analyzed by flow cytometry. The figures represent the consolidated data of at least n = 8 independent experiments. The Wilcoxon test was used for comparisons between groups.

markedly reduced FSC and increased SSC. It is important to note the presence of U937 cells with a lower DNA content (hypoploidy).

4. Discussion

The iron oxide nanoparticles can be used as contrast agents in Magnetic Resonance Imaging (MRI) due to their superparamagnetic properties that have been well characterized in previous reviews [47]. The use of this tool for taking images has the advantage of reaching difficultly accessible tissues in a non-invasive way. This type of imaging has been implemented [48] and is proposed as a diagnostic tool that allows a more effective characterization of tissue or vascular lesions; even it could differentiate cellular subtypes in inflammatory infiltrates, contributing this way to a better understanding of the biology of several pathologies [49].

4.1. Platelet activation and aggregation

Patients with atherosclerosis, coronary artery disease, cerebrovascular disease, peripheral arterial disease, acute coronary syndrome, or percutaneous coronary interventions, will certainly require diagnostic tests like MRI. They are candidates for the use of contrast agents due to the problematic characterization of their tissue injuries by non-invasive procedures. However, these patients commonly present platelet hyperreactivity [50] and functional alterations in leukocytes. For this reason, it is essential to evaluate the biocompatibility of nanoparticles and their coatings with platelets and cells of the immune system.

In some cases, nanoparticles have induced accelerated platelet aggregation [51,52]. Platelets express membrane SRs as CD36, SR-B1 and LOX-1 [38]; CD36 and SR-B1 can participate in their hyperreactivity [53]. These SRs can interact with negatively charged ligands as the polyacrylate present in the nanoparticles' coating [1]. Therefore, the study of the activation and aggregation of platelets when in contact with PAC-IONs was proposed as an initial characterization of their biocompatibility. Biocompatibility is one of the ten criteria that nanomaterials with a potential biomedical application should meet according to the guidelines of The National Institute of Health of the United States [54].

PMA, AA, and ADP were used to induce platelet activation and aggregation. PMA is a thrombin receptor agonist [55], AA induces aggregation via thromboxane A2 receptor and prostaglandin H2 [56], and ADP induces aggregation through the purinergic receptors [57]. The PAC-IONs did not induce either activation or aggregation of platelets but did antagonize the AA and PMA-induced aggregation. Polyacrylate accelerates the antithrombin activity [58], and a report suggested that it binds antithrombin in both the pentasaccharide- and the extended heparin-binding site, forming ionic interactions that inhibit thrombin [58]. The finding that PAC-IONs did not induce platelet activation and aggregation is essential from the point of view of biocompatibility of the material and their basic characterization as nanosensors.

4.2. Phagocytic capacity of MDMs differentiated in the presence of PAC-IONs

The removal of ACs, mainly executed by mononuclear phagocytes, is part of the homeostasis and generally does not trigger an inflammatory response [59]. The removal of ACs is linked to the surface

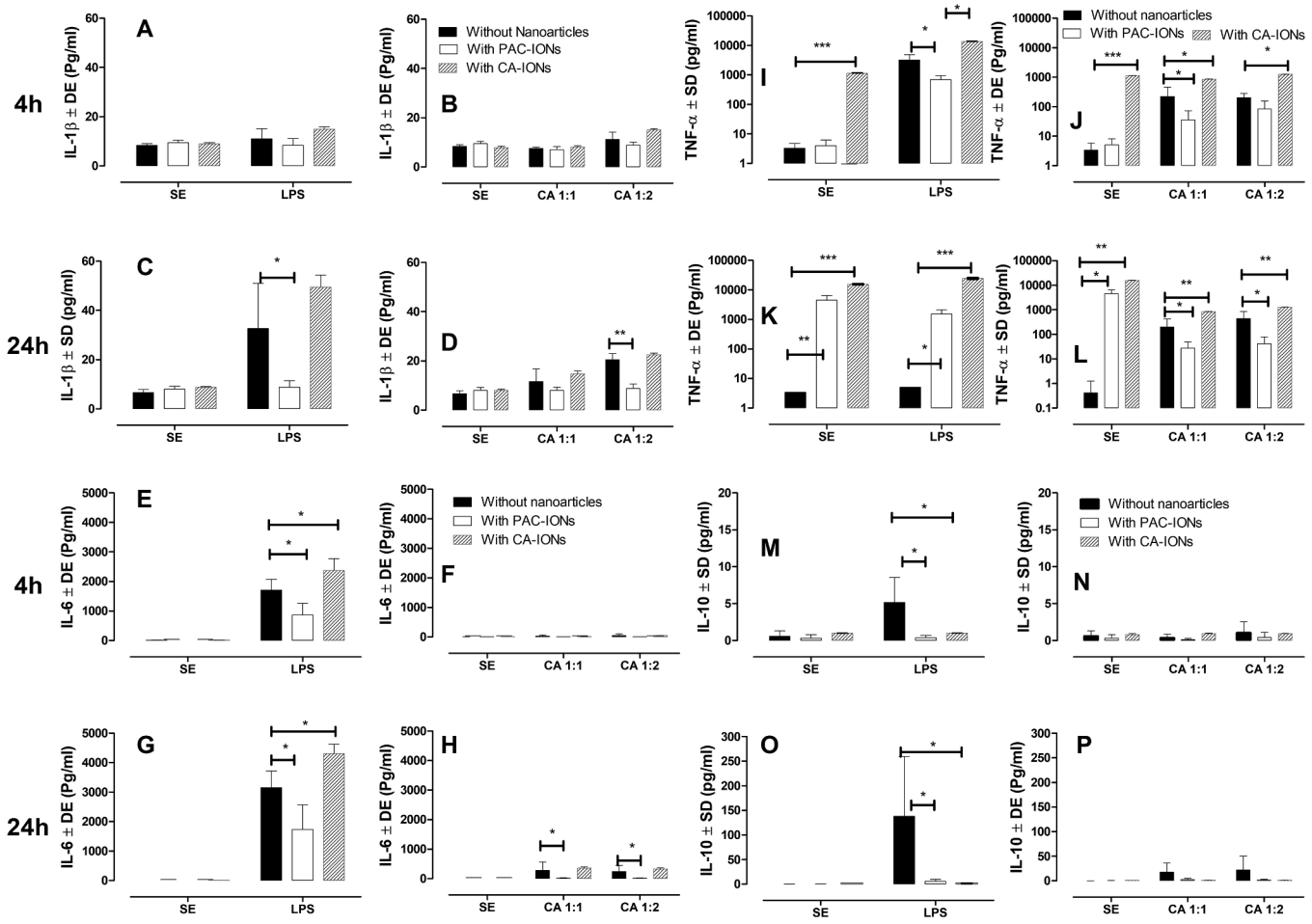

Fig. 6. Levels of cytokines in cultures of MDMs differentiated in the presence of PAC-IONs and CA-IONs and stimulated with LPS or ACs. MDMs were differentiated in the absence (black bars) or presence of PAC-IONs (white bars) or CA-IONs (hatched bars) for 120 h. Then, they were stimulated with LPS or ACs at 1:1 and 1:2 ratios (MDM: AC) and supernatants were collected for quantification of cytokines. The bars represent the Mean ± the standard deviation values for IL-1β (A-D), IL-6 (E-H), TNF-α (I-L), and IL-10 (M-P) in supernatants collected at 4 and 24 h after stimulation. Comparisons were made with a two-way ANOVA with a Bonferroni post-test. n = 4 independent experiments. $^{*}p < 0.05$ and $^{**}p < 0.01$.

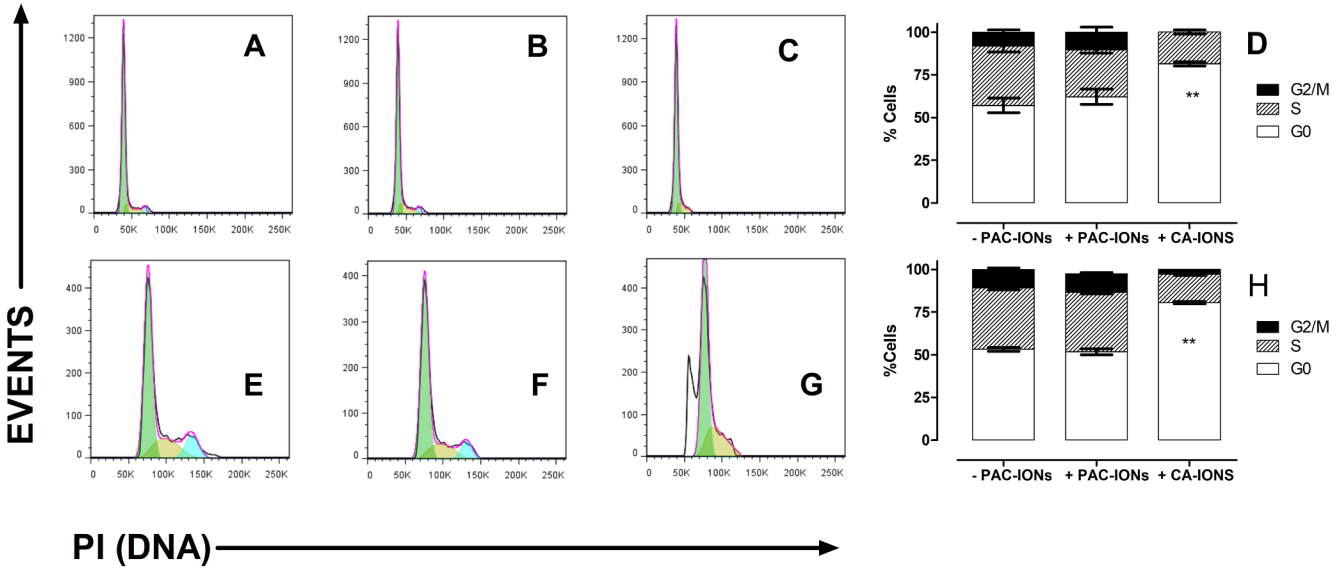

Fig. 7. Effect of PAC-IONs on the cell cycle of Jurkat (A-D) and U937 (E-H) cells. Jurkat and U937 cells were cultured for 72 h in the absence (A and E) or presence (B and F) of PAC-IONs or CA-IONs (C and G). The cells were fixed with ethanol and stained with PI/RNase A and analyzed by flow cytometry under the Dean-Jett-Fox model (A-C, and E-G) that was fixed using the FlowJo software. The proportions of cells in each phase of the cell cycle were compared using the Mann-Whitney *U* test (D and H).

exposure and release of mediators that usually are only present during cellular senescence and death [60]. Different autoimmune pathologies are characterized by a deficient removal of ACs, although the genetic background of the individual and some external factors also participate in the process. For example, in the case of a patient with an autoimmune disease, and tissue damage –atheromatous plaques, lupus nephritis, injured synovium [59]– because the removal of ACs would take longer than normal, resulting in a secondary necrosis, accumulation of micro-particles, oxidative modifications as citrullination [60], and HMGB1 exposure [61,62]. The HMGB1 from these apoptotic cells reduces phagocytosis by binding and masking phosphatidylserine by neutrophils and by binding to the phagocyte αvβ3 integrin [62]. All of these events steadily increases the availability of cellular debris to form neoantigens. In turn, they give rise to immune complexes that are involved in tissue damage: immune complexes grow in size and complexity, deposit in tissues, and activate the complement system [63].

The SRs also have the capacity to bind oxidized and acetylated lipoproteins, which competitively inhibit the endocytosis of polyacrylate-conjugated liposomes [1]. The fact that polyacrylate is the coating of the particles here studied, allows us to propose a possible interaction of the PAC-IONs with the SRs. Nevertheless, we observed that phagocytosis of latex beads was not affected; therefore, the phagocytosis of ACs was also studied. Although phagocytosis of ACs was not affected, the number of cells phagocytosed by MDM did decrease. It is still unclear if a potential interaction of PAC-IONs with the SRs could reduce the ingestion capacity of phagocytes. To this purpose, competition tests involving specific ligands or blocking antibodies of phagocytoses are required.

It should be noted that the hypotheses and tests here exposed were based on the nature of the nanoparticle coating because previous observations from our group showed that the entrance and cytotoxicity of the nanoparticles depend on their coating. However, the coating is not always critical for the interaction with cells [64].

4.3. PAC-IONs did not change the cytokine profile of MDMs in culture but did reduce the levels of some cytokines

We found that MDMs differentiated in the presence of PAC-IONs increase the synthesis of TNF-α. This finding agrees with previous publications of monocytes exposed to Fe_3O_4 and Fe_2O_3 nanoparticles [65]. The increase in TNF-α has been attributed to the fact that metal nanoparticles can release ions that alter the expression of TLRs and increase the proinflammatory response of macrophages [66]. On the contrary, in other studies, TNF-α was not induced in macrophages exposed to carboxydextran-coated IONs; the authors proposed that it could be attributed to lysosomal enzymes that degrade the coating of the nanoparticles; this way, the exposed iron oxide core could catalyze the generation of reactive oxygen species (ROS) [67]. ROS can damage cellular proteins, lipids, nucleic acids and components of the extracellular matrix through the donation of electrons resulting in lipid peroxidation, enzyme dysfunction and the promotion of pro-inflammatory signals [68]. This event could be one of the mechanisms that explain the increased level of TNF-α in unstimulated cultures and the lower levels of cytokines in cultures of MDMs differentiated in the presence of PAC-IONs.

Previous studies evaluated the response to LPS of peritoneal macrophages from C57BL/6 mice and Lewis rats previously exposed to carboxydextran-coated superparamagnetic iron oxide (SPIO) and ultrasmall superparamagnetic iron oxide (USPIO) particles. Mouse macrophages exposed to SPIO and USPIO particles produced IL-10 that increased when stimulated with LPS. However, there was not any effect on TNF-α. On the contrary, rat macrophages treated with SPIO and USPIO decreased the production of TNF-α even in the presence of LPS, slightly decreased IL-10, and did not change the basal levels of TGF-β and IL-12p40. These results evidenced that the endocytosis of these particles changed the macrophages towards an anti-inflammatory phenotype, and lower the response to the proinflammatory stimuli [69]. Similarly, in the present study, the human MDMs differentiated in the presence of PAC-IONs showed a decreased level of TNF-α after treatment with LPS at 24 h. These pieces of evidence show that the responses of phagocytes vary depending on the type of the cells.

Previous studies showed that the contrast agent Endorem® (iron oxide nanoparticles) changes the production of cytokines by MDMs. These cells when treated for three days with low (25–50 μg mL) or high doses (75–100 μg/mL) of Endorem®, increased and decreased the production of cytokines, respectively. This finding, in conjunction with results in rats and mice, allowed Endorem® to be patented for the treatment of noninfectious inflammatory disorders [70]. That research considered the effect of nanoparticles on the production of cytokines by MDMs, in contrast to our study, in which, the main objective was to evaluate the effects of PAC-IONs during the differentiation of monocytes to macrophages. The decreased level of cytokines found in the present study is similar to the results observed with high doses of Endorem®, but there is not a clear explanation about it. Finally, we do not know the potential *in vivo* effects of PAC-IONs and whether the alterations they caused in the cell functional characteristics would be transitory or definitive. Therefore, more studies are required to guarantee the use of PAC-IONs as innocuous nanosensors.

4.4. Comparison of PAC-IONs with a commercial source of iron nanoparticles

We could not find polyacrylate-coated nanoparticles commercially available. Nevertheless, the most similar particles we found (in terms of size and physical properties) were the CA-IONs included in this study. Some groups have tested nanoparticles with carboxylic acid in the shells for their biosafety characteristics. Nonetheless, those coats have amphiphilic structure including a hydrophobic hyperbranched polyester (HBPE) core and hydrophilic carboxylated terminal groups [71], which should make them biologically different from CA-IONs. For the present bioassays, we used an equivalent amount of iron for both particle preparations, but commercial CA-IONs induced platelet aggregation, an in addition to the decrease in CD36 that was observed with PAC-IONs also reduced HLA-DR expression in MDMs. These nanoparticles compromised more extensively the functions of MDMs; namely, they reduced the uptake of apoptotic bodies, increased the proinflammatory cytokines IL-1ß, IL-6, and TNF-a with a concomitant reduction of IL-10 in either the presence of LPS or apoptotic cells. Besides, the CA-IONs induced an arrest of the cell cycle in both Jurkat and U937 cell lines, emphasizing the lack of cell specificity. All these evidences suggest that in-house synthesized PAC-IONs demonstrated to have biosafety features in our *in vitro* system.

Acknowledgments

This study is part of the project entitled "*Functionalization of magnetic iron oxide nanoparticles as a potential tool for tracking of tissue damage*." Supported by the Comité para el Desarrollo de la Investigación (Committee for Development of Research/CODI by its acronym in Spanish) Project 2560. The electromagnetic separation services were financed by the CODI call 2013-2, through the Research Center of the Facultad de Ciencias Exactas y Naturales and the Programa de Sostenibilidad (Sustainability Program) call 2012-2014 for the Cell Immunology and Immunogenetics Group at Universidad de Antioquia. We also thank Dr. Marta Mesa for her English Language Wording, detailed review, and correction.

Author contributions

M.GV. – study concept, experimental design, acquisition, analysis, interpretation of data, and drafting of the manuscript; M.T.C. – data acquisition, analysis, and interpretation of data; B.L.O.R. – experiments

for the second submission of the manuscript; J.U. – Nanoparticle preparation, nanoparticle quality analysis, and interpretation of data; E.Y.T. – data acquisition, analysis, and interpretation of data; O.L.A.O. – Nanoparticle preparation, nanoparticle quality analysis and interpretation of data, study concept, and experimental design; M.R. – study concept, experimental design, flow cytometry acquisition, cell sorting, analysis, and interpretation of data, drafting of the manuscript and supervision. We also thank Dr. Marta Mesa for their English Language Wording review, editing and correction.

Appendix A. Supplementary data

Supplementary data to this article can be found online at https://doi.org/10.1016/j.cellimm.2019.03.005.

References

[1] M. Fujiwara, J.D. Baldeschwieler, R.H. Grubbs, Receptor-mediated endocytosis of poly(acrylic acid)-conjugated liposomes by macrophages, Biochim. Biophys. Acta 1278 (1996) 59–67.
[2] L. Ziegler-Heitbrock, P. Ancuta, S. Crowe, M. Dalod, V. Grau, D.N. Hart, P.J. Leenen, Y.J. Liu, G. MacPherson, G.J. Randolph, J. Scherberich, J. Schmitz, K. Shortman, S. Sozzani, H. Strobl, M. Zembala, J.M. Austyn, M.B. Lutz, Nomenclature of monocytes and dendritic cells in blood, Blood 116 (2010) e74–e80.
[3] W. Vermi, A. Micheletti, G. Finotti, C. Tecchio, F. Calzetti, S. Costa, M. Bugatti, S. Calza, C. Agostinelli, S. Pileri, P. Balzarini, A. Tucci, G. Rossi, L. Furlani, G. Todeschini, A. Zamo, F. Facchetti, L. Lorenzi, S. Lonardi, M.A. Cassatella, slan (+) Monocytes and macrophages mediate CD20-dependent B-cell lymphoma elimination via ADCC and ADCP, Cancer Res. 78 (2018) 3544–3559.
[4] P. Ancuta, A slan-based nomenclature for monocytes? Blood 126 (2015) 2536–2538.
[5] T.P. Hofer, A.M. Zawada, M. Frankenberger, K. Skokann, A.A. Satzl, W. Gesierich, M. Schuberth, J. Levin, A. Danek, B. Rotter, G.H. Heine, L. Ziegler-Heitbrock, slan-defined subsets of CD16-positive monocytes: impact of granulomatous inflammation and M-CSF receptor mutation, Blood 126 (2015) 2601–2610.
[6] S. Ahmad, M.J. Cudmore, K. Wang, P. Hewett, R. Potluri, T. Fujisawa, A. Ahmed, Angiopoietin-1 induces migration of monocytes in a tie-2 and integrin-independent manner, Hypertension 56 (2010) 477–483.
[7] N. Figueroa-Vega, M. Alfonso-Perez, C. Cuesta-Mateos, F. Sanchez-Madrid, R. Moreno-Otero, R. Gonzalez-Amaro, M. Marazuela, Tie-2 is overexpressed by monocytes in autoimmune thyroid disorders and participates in their recruitment to the thyroid gland, J. Clin. Endocrinol. Metab. 94 (2009) 2626–2633.
[8] C. Murdoch, S. Tazzyman, S. Webster, C.E. Lewis, Expression of Tie-2 by human monocytes and their responses to angiopoietin-2, J. Immunol. 178 (2007) 7405–7411.
[9] M. Rojas, M. Olivier, L.F. Garcia, Activation of JAK2/STAT1-alpha-dependent signaling events during Mycobacterium tuberculosis-induced macrophage apoptosis, Cell. Immunol. 217 (2002) 58–66.
[10] M. Rojas, L.F. Garcia, J. Nigou, G. Puzo, M. Olivier, Mannosylated lipoarabinomannan antagonizes Mycobacterium tuberculosis-induced macrophage apoptosis by altering Ca+2-dependent cell signaling, J. Infect. Dis. 182 (2000) 240–251.
[11] M. Rojas, L.F. Barrera, G. Puzo, L.F. Garcia, Differential induction of apoptosis by virulent Mycobacterium tuberculosis in resistant and susceptible murine macrophages: role of nitric oxide and mycobacterial products, J. Immunol. 159 (1997) 1352–1361.
[12] M. Rojas, L.F. Barrera, L.F. Garcia, Induction of apoptosis in murine macrophages by Mycobacterium tuberculosis is reactive oxygen intermediates-independent, Biochem. Biophys. Res. Commun. 247 (1998) 436–442.
[13] H. Pan, B.S. Yan, M. Rojas, Y.V. Shebzukhov, H. Zhou, L. Kobzik, D.E. Higgins, M.J. Daly, B.R. Bloom, I. Kramnik, Ipr1 gene mediates innate immunity to tuberculosis, Nature 434 (2005) 767–772.
[14] D.P. Gil, L.G. Leon, L.I. Correa, J.R. Maya, S.C. Paris, L.F. Garcia, M. Rojas, Differential induction of apoptosis and necrosis in monocytes from patients with tuberculosis and healthy control subjects, J. Infect. Dis. 189 (2004) 2120–2128.
[15] M.D. Sanchez, Y. Garcia, C. Montes, S.C. Paris, M. Rojas, L.F. Barrera, M.A. Arias, L.F. Garcia, Functional and phenotypic changes in monocytes from patients with tuberculosis are reversed with treatment, Microbes Infect. 8 (2006) 2492–2500.
[16] D. Castano, L.F. Garcia, M. Rojas, Increased frequency and cell death of CD16+ monocytes with Mycobacterium tuberculosis infection, Tuberculosis 91 (2011) 348–360.
[17] M.E. Ramirez-Agudelo, A.C. Caro, C.A. Jaramillo, M. Rojas, Fatty acid profile during the differentiation and infection with Mycobacterium tuberculosis of mononuclear phagocytes of patients with TB and healthy individuals, Cell. Immunol. 270 (2011) 145–155.
[18] D. Strauss-Ayali, S.M. Conrad, D.M. Mosser, Monocyte subpopulations and their differentiation patterns during infection, J. Leukoc. Biol. 82 (2007) 244–252.
[19] C. Shi, E.G. Pamer, Monocyte recruitment during infection and inflammation, Nat. Rev. Immunol. 11 (2011) 762–774.
[20] A. Puchner, V. Saferding, M. Bonelli, Y. Mikami, M. Hofmann, J.S. Brunner, M. Caldera, E. Goncalves-Alves, N.B. Binder, A. Fischer, E. Simader, C.W. Steiner, H. Leiss, S. Hayer, B. Niederreiter, T. Karonitsch, M.I. Koenders, B.K. Podesser, J.J. O'Shea, J. Menche, J.S. Smolen, K. Redlich, S. Bluml, Non-classical monocytes as mediators of tissue destruction in arthritis, Ann. Rheum. Dis. (2018).
[21] K. Buscher, P. Marcovecchio, C.C. Hedrick, K. Ley, Patrolling mechanics of non-classical monocytes in vascular inflammation, Front. Cardiovasc. Med. 4 (2017) 80.
[22] L. Ziegler-Heitbrock, The CD14+ CD16+ blood monocytes: their role in infection and inflammation, J. Leukoc. Biol. 81 (2007) 584–592.
[23] J. Noll, E. Helk, H. Fehling, H. Bernin, C. Marggraff, T. Jacobs, S. Huber, P. Pelczar, T. Ernst, H. Ittrich, B. Otto, H.W. Mittrucker, C. Holscher, F. Tacke, I. Bruchhaus, E. Tannich, H. Lotter, IL-23 prevents IL-13-dependent tissue repair associated with Ly6C(lo) monocytes in Entamoeba histolytica-induced liver damage, J. Hepatol. 64 (2016) 1147–1157.
[24] A. Kaufmann, B. Musset, S.H. Limberg, V. Renigunta, R. Sus, A.H. Dalpke, K.M. Heeg, B. Robaye, P.J. Hanley, "Host tissue damage" signal ATP promotes non-directional migration and negatively regulates toll-like receptor signaling in human monocytes, J. Biol. Chem. 280 (2005) 32459–32467.
[25] D.I. Rosenthal, C.R. Becerra, R.D. Toto, D.P. Carbone, E.P. Frenkel, Reversible renal toxicity resulting from high single doses of the new radiosensitizer gadolinium texaphyrin, Am. J. Clin. Oncol. 23 (2000) 593–598.
[26] A. Spencer, S. Wilson, E. Harpur, Gadolinium chloride toxicity in the mouse, Hum. Exp. Toxicol. 17 (1998) 633–637.
[27] D.R. Koop, B. Klopfenstein, Y. Iimuro, R.G. Thurman, Gadolinium chloride blocks alcohol-dependent liver toxicity in rats treated chronically with intragastric alcohol despite the induction of CYP2E1, Mol. Pharmacol. 51 (1997) 944–950.
[28] A.J. Spencer, S.A. Wilson, J. Batchelor, A. Reid, J. Rees, E. Harpur, Gadolinium chloride toxicity in the rat, Toxicol. Pathol. 25 (1997) 245–255.
[29] R.A. Ball, G. Van Gelder, Chronic toxicity of gadolinium oxide for mice following exposure by inhalation, Arch. Environ. Health 13 (1966) 601–608.
[30] M.A. Perazella, Current status of gadolinium toxicity in patients with kidney disease, Clin. J. Am. Soc. Nephrol. 4 (2009) 461–469.
[31] M.A. Perazella, Gadolinium-contrast toxicity in patients with kidney disease: nephrotoxicity and nephrogenic systemic fibrosis, Curr. Drug Saf. 3 (2008) 67–75.
[32] S. Sakamoto, K. Eguchi, M. Shibukawa, Y. Kiura, F. Yamasaki, Y. Kajiwara, T. Matsushige, K. Kurisu, Cerebral angiography using gadolinium as an alternative contrast medium in a patient with severe allergy to iodinated contrast medium, Hiroshima J. Med. Sci. 59 (2010) 15–16.
[33] Y. Safriel, M. Ali, M. Hayt, R. Ang, Gadolinium use in spine procedures for patients with allergy to iodinated contrast–experience of 127 procedures, AJNR Am. J. Neuroradiol. 27 (2006) 1194–1197.
[34] D. Noorhasan, M.J. Heard, Gadolinium radiologic contrast is a useful alternative for hysterosalpingography in patients with iodine allergy, Fertil. Steril. 84 (2005) 1744.
[35] H. Sasamura, S. Hashimoto, S. Kuribayashi, K. Ueno, A. Takase, M. Hayashi, T. Saruta, Use of gadolinium contrast adrenal venography for the assessment of primary aldosteronism in a patient with iodine allergy, Endocr. J. 51 (2004) 487–492.
[36] F.J. Falco, J.G. Moran, Lumbar discography using gadolinium in patients with iodine contrast allergy followed by postdiscography computed tomography scan, Spine (Phila Pa 1976) 28 (2003) E1–E4.
[37] G. Brix, E.A. Nekolla, D. Nosske, J. Griebel, Risks and safety aspects related to PET/MR examinations, Eur. J. Nucl. Med. Mol. Imaging 36 (Suppl. 1) (2009) S131–S138.
[38] J.E. Murphy, P.R. Tedbury, S. Homer-Vanniasinkam, J.H. Walker, S. Ponnambalam, Biochemistry and cell biology of mammalian scavenger receptors, Atherosclerosis 182 (2005) 1–15.
[39] C.L. Lin, C.F. Lee, W.Y. Chiu, Preparation and properties of poly(acrylic acid) oligomer stabilized superparamagnetic ferrofluid, J. Colloid Interface Sci. 291 (2005) 411–420.
[40] X. Li, A. Radomski, O.I. Corrigan, L. Tajber, F. De Sousa Menezes, S. Endter, C. Medina, M.W. Radomski, Platelet compatibility of PLGA, chitosan and PLGA-chitosan nanoparticles, Nanomedicine (Lond) 4 (2009) 735–746.
[41] J. Yourno, J. Walsh, G. Kornatowski, D. O'Connor, S.A. Kumar, Nonspecific esterases of leukemia cell lines: evidence for activation of myeloid-associated zymogens in HL-60 by phorbol esters, Blood 63 (1984) 238–241.
[42] P. Pozarowski, Z. Darzynkiewicz, Analysis of cell cycle by flow cytometry, Methods Mol. Biol. 281 (2004) 301–311.
[43] M. Settles, M. Etzrodt, K. Kosanke, M. Schiemann, A. Zimmermann, R. Meier, R. Braren, A. Huber, E.J. Rummeny, R. Weissleder, F.K. Swirski, M. Wildgruber, Different capacity of monocyte subsets to phagocytose iron-oxide nanoparticles, PLoS ONE 6 (2011) e25197.
[44] D. Castano, L.F. Barrera, M. Rojas, Mycobacterium tuberculosis alters the differentiation of monocytes into macrophages in vitro, Cell. Immunol. 268 (2011) 60–67.
[45] R.R. Johnson-Tidey, J.L. McGregor, P.R. Taylor, R.N. Poston, Increase in the adhesion molecule P-selectin in endothelium overlying atherosclerotic plaques. Coexpression with intercellular adhesion molecule-1, Am. J. Pathol. 144 (1994) 952–961.
[46] L.M. Yassin, M. Rojas, L.A. Ramirez, L.F. Garcia, G. Vasquez, Monocyte activation by apoptotic cells removal in systemic lupus erythematosus patients, Cell. Immunol. 266 (2010) 52–60.
[47] J.W. Bulte, D.L. Kraitchman, Iron oxide MR contrast agents for molecular and cellular imaging, NMR Biomed. 17 (2004) 484–499.
[48] C. Felton, A. Karmakar, Y. Gartia, P. Ramidi, A.S. Biris, A. Ghosh, Magnetic nanoparticles as contrast agents in biomedical imaging: recent advances in iron- and manganese-based magnetic nanoparticles, Drug Metab. Rev. 46 (2014) 142–154.
[49] M. Lech, H.J. Anders, Macrophages and fibrosis: How resident and infiltrating

mononuclear phagocytes orchestrate all phases of tissue injury and repair, Biochim. Biophys. Acta 2013 (1832) 989–997.
[50] M. Valiyaveettil, E.A. Podrez, Platelet hyperreactivity, scavenger receptors and atherothrombosis, J. Thromb. Haemost. 7 (Suppl. 1) (2009) 218–221.
[51] C.F. Jones, R.A. Campbell, A.E. Brooks, S. Assemi, S. Tadjiki, G. Thiagarajan, C. Mulcock, A.S. Weyrich, B.D. Brooks, H. Ghandehari, D.W. Grainger, Cationic PAMAM dendrimers aggressively initiate blood clot formation, ACS Nano 6 (2012) 9900–9910.
[52] M.A. Cejas, C. Chen, W.A. Kinney, B.E. Maryanoff, Nanoparticles that display short collagen-related peptides. Potent stimulation of human platelet aggregation by triple helical motifs, Bioconjug. Chem. 18 (2007) 1025–1027.
[53] P.F. Bray, Platelet hyperreactivity: predictive and intrinsic properties, Hematol. Oncol. Clin. North Am. 21 (633–645) (2007) v–vi.
[54] M.A. Dobrovolskaia, P. Aggarwal, J.B. Hall, S.E. McNeil, Preclinical studies to understand nanoparticle interaction with the immune system and its potential effects on nanoparticle biodistribution, Mol. Pharm. 5 (2008) 487–495.
[55] J. Zhang, J. Zhang, S.J. Shattil, M.C. Cunningham, S.E. Rittenhouse, Phosphoinositide 3-kinase gamma and p85/phosphoinositide 3-kinase in platelets. Relative activation by thrombin receptor or beta-phorbol myristate acetate and roles in promoting the ligand-binding function of alphaIIbbeta3 integrin, J. Biol. Chem. 271 (1996) 6265–6272.
[56] L.V. Parise, D.L. Venton, G.C. Le Breton, Arachidonic acid-induced platelet aggregation is mediated by a thromboxane A2/prostaglandin H2 receptor interaction, J. Pharmacol. Exp. Ther. 228 (1984) 240–244.
[57] S. Murugappa, S.P. Kunapuli, The role of ADP receptors in platelet function, Front. Biosci. 11 (2006) 1977–1986.
[58] B.H. Monien, K.I. Cheang, U.R. Desai, Mechanism of poly(acrylic acid) acceleration of antithrombin inhibition of thrombin: implications for the design of novel heparin mimics, J. Med. Chem. 48 (2005) 5360–5368.
[59] I.K. Poon, C.D. Lucas, A.G. Rossi, K.S. Ravichandran, Apoptotic cell clearance: basic biology and therapeutic potential, Nat. Rev. Immunol. 14 (2014) 166–180.
[60] K.D. Kenyon, C. Cole, F. Crawford, J.W. Kappler, J.M. Thurman, D.L. Bratton, S.A. Boackle, P.M. Henson, IgG autoantibodies against deposited C3 inhibit macrophage-mediated apoptotic cell engulfment in systemic autoimmunity, J. Immunol. 187 (2011) 2101–2111.
[61] K.R. Zettel, M. Dyer, J.S. Raval, X. Wu, J.R. Klune, A. Gutierrez, D.J. Triulzi, T.R. Billiar, M.D. Neal, Aged human stored red blood cell supernatant inhibits macrophage phagocytosis in an HMGB1 dependent manner after trauma in a murine model, Shock 47 (2017) 217–224.
[62] A. Friggeri, Y. Yang, S. Banerjee, Y.J. Park, G. Liu, E. Abraham, HMGB1 inhibits macrophage activity in efferocytosis through binding to the alphavbeta3-integrin, Am. J. Physiol. Cell Physiol. 299 (2010) C1267–C1276.
[63] S. Jancar, M. Sanchez Crespo, Immune complex-mediated tissue injury: a multistep paradigm, Trends Immunol. 26 (2005) 48–55.
[64] Y. Chao, P.P. Karmali, R. Mukthavaram, S. Kesari, V.L. Kouznetsova, I.F. Tsigelny, D. Simberg, Direct recognition of superparamagnetic nanocrystals by macrophage scavenger receptor SR-AI, ACS Nano 7 (2013) 4289–4298.
[65] A.L. Guildford, T. Poletti, L.H. Osbourne, A. Di Cerbo, A.M. Gatti, M. Santin, Nanoparticles of a different source induce different patterns of activation in key biochemical and cellular components of the host response, J. R. Soc. Interface 6 (2009) 1213–1221.
[66] M. Lucarelli, A.M. Gatti, G. Savarino, P. Quattroni, L. Martinelli, E. Monari, D. Boraschi, Innate defence functions of macrophages can be biased by nano-sized ceramic and metallic particles, Eur. Cytokine Netw. 15 (2004) 339–346.
[67] O. Lunov, T. Syrovets, B. Buchele, X. Jiang, C. Rocker, K. Tron, G.U. Nienhaus, P. Walther, V. Mailander, K. Landfester, T. Simmet, The effect of carboxydextran-coated superparamagnetic iron oxide nanoparticles on c-Jun N-terminal kinase-mediated apoptosis in human macrophages, Biomaterials 31 (2010) 5063–5071.
[68] V. Temkin, M. Karin, From death receptor to reactive oxygen species and c-Jun N-terminal protein kinase: the receptor-interacting protein 1 odyssey, Immunol. Rev. 220 (2007) 8–21.
[69] I. Siglienti, M. Bendszus, C. Kleinschnitz, G. Stoll, Cytokine profile of iron-laden macrophages: implications for cellular magnetic resonance imaging, J. Neuroimmunol. 173 (2006) 166–173.
[70] Y. Amsalem, Y. Mardor, M.S. Feinberg, N. Landa, L. Miller, D. Daniels, A. Ocherashvilli, R. Holbova, O. Yosef, I.M. Barbash, J. Leor, Iron-oxide labeling and outcome of transplanted mesenchymal stem cells in the infarcted myocardium, Circulation 116 (2007) I38–I45.
[71] Q. Han, X. Chen, W. Wang, W. Zhao, K. Wang, B. Wang, J. Shen, Preparation and biosafety assessment of water-soluble hyperbranched polyester nanoparticles with carboxylic acid functional groups, J. Nanosci. Nanotechnol. 15 (2015) 138–143.